

Provided for non-commercial research and education use.  
Not for reproduction, distribution or commercial use.



This article appeared in a journal published by Elsevier. The attached copy is furnished to the author for internal non-commercial research and education use, including for instruction at the authors institution and sharing with colleagues.

Other uses, including reproduction and distribution, or selling or licensing copies, or posting to personal, institutional or third party websites are prohibited.

In most cases authors are permitted to post their version of the article (e.g. in Word or Tex form) to their personal website or institutional repository. Authors requiring further information regarding Elsevier's archiving and manuscript policies are encouraged to visit:

<http://www.elsevier.com/authorsrights>



Contents lists available at ScienceDirect

## Experimental Thermal and Fluid Science

journal homepage: [www.elsevier.com/locate/etfs](http://www.elsevier.com/locate/etfs)

# Experimental study of the thermal behavior of spark generated bubbles in water

Karel Vokurka<sup>a,\*</sup>, Jaroslav Plocek<sup>b</sup><sup>a</sup> Physics Department, Technical University of Liberec, Studentská 2, 461 17 Liberec, Czech Republic<sup>b</sup> Physics Department, Czech Technical University in Prague, Faculty of Electrical Engineering, Technická 2, 166 00 Praha 6, Czech Republic

## ARTICLE INFO

## Article history:

Received 7 March 2013

Received in revised form 10 July 2013

Accepted 12 July 2013

Available online 20 July 2013

## Keywords:

Thermal behavior of bubbles

Spark bubbles

Cavitation

Discharges in water

## ABSTRACT

In the paper thermal behavior of spark generated bubbles is studied experimentally using an optic sensor (a photodiode) and an acoustic sensor (a hydrophone). It is shown that there is plasma in the bubble interior during the whole first bubble oscillation. A simple method is used, based on several assumptions, which allows determining an estimate of the radiated optic energy and from it the surface temperature of the bubble when the thermal radiation reaches its maximum. This temperature can be then exploited when computing a number of other quantities. An example of the energy partition in the first bubble growth phase and in the first compression and the following expansion phases is given. The estimate of the surface plasma temperature when the bubble is compressed to its first minimum volume is also given and it has been found to be approximately 5900 K in a selected experiment. It is also shown that spark generated bubbles do not behave adiabatically and that the plasma in the bubble interior represents a highly non-homogeneous medium far from an equilibrium state, for which the equation of the state of an ideal gas cannot be used.

© 2013 Elsevier Inc. All rights reserved.

## 1. Introduction

Oscillations of bubbles in liquids have been intensively studied for many decades. An overview of these works is given in Refs. [1,2]. Recent efforts in research of oscillating bubbles are aiming at medical applications, such as contrast-enhancing in medical ultrasonic imaging or ultrasound mediated drug delivery with micro-bubbles [3–7], at chemical production of radicals inside acoustically driven bubbles [8], at hydrodynamic load reducing effects [9], and to the effect of internal structure on the behavior of spherical implodable volumes [10]. Laser induced chemical reactions that produce bubbles have also been recently studied [11].

In spite of many works dealing with thermal behavior of bubbles (see, for example Refs. [12–18]), and a recent review of works dealing with thermal damping [19]), this problem has not been satisfactorily clarified yet. The reason is a great complexity of bubble thermal behavior and its dependence on many different factors. For example, heat losses might depend on bubble oscillation intensity, on bubble size, on the content of the bubble interior, and on the bubble excitation technique, to name just the most important factors.

As far as the bubble oscillation intensity is concerned, most of the experimental data related to the thermal behavior have been

\* Corresponding author. Tel.: +420 485 353 401.

E-mail addresses: [karel.vokurka@tul.cz](mailto:karel.vokurka@tul.cz) (K. Vokurka), [plocek@fel.cvut.cz](mailto:plocek@fel.cvut.cz) (J. Plocek).

obtained when studying low intensity bubble oscillations [12,17]. Unfortunately, no work has been published yet in which the thermal behavior of bubbles oscillating with high intensity has been studied experimentally. For example, in a recent relatively extensive review [20] there is no explicit mention concerning the thermal behavior of the spark and laser generated bubbles and the authors assume implicitly that laser generated bubbles always behave adiabatically (see bubble models presented in Section 2 of Ref. [20]).

When considering the influence of bubble sizes on their thermal behavior, small bubbles are believed to behave isothermally and large bubbles adiabatically [12,14]. Oscillations of bubbles having an intermediate size are then expected to be accompanied by heat losses [12,14]. Unfortunately, only rough estimates of the limiting bubble sizes, for which isothermal or adiabatic behavior can be expected, have been given in literature and these estimates have been obtained only for low intensities of bubble oscillations [12,14]. As far as the bubble content is concerned, in a somewhat simplified way it can be assumed that the bubbles contain either gas or vapor in their interior [21]. And again, all the experimental data have been obtained for gas bubbles only. Finally, a relation between different excitation techniques and the corresponding bubble thermal behavior has not been studied at all yet.

The thermal behavior of the bubbles will certainly be influenced by several physical processes. First, it is the heat flow between the bubble interior and the surrounding liquid. Second, it can be evaporation and condensation at the bubble liquid interface. And third,

in some situations, it can be thermal radiation from the bubble interior into the surrounding liquid. The thermal radiation is important for spark and laser generated bubbles first of all. Examples of theoretical computations concerning thermal radiation losses can be found in Refs. [22–24]. However, computations in Refs. [22,23] are limited to a time interval immediately following the discharge or laser irradiation of the liquid. Later times of bubble oscillations have been considered only in Ref. [24].

In earlier experiments [25,26] oscillating bubbles have been generated by spark discharges. In this way relatively large bubbles have been obtained, with maximum radii ranging from about 18 mm to 55 mm. As a very intensive light emission from these bubbles has been observed, a relatively simple experimental setup has been prepared to examine this phenomenon in a greater detail. This setup is described in the following section. Although the results obtained are more or less qualitative only, their analysis yields a useful insight into the complex phenomenon of spark bubble thermal behavior. And even if the analysis given here is valid for spark generated bubbles only, the results may be useful even when studying other types of bubbles. The work reported here has been presented in a shortened form at a conference [27].

## 2. Experimental setup

Freely oscillating bubbles have been generated by means of discharging a capacitor bank via a sparker submerged in water in a laboratory tank having dimensions of 6 m (length)  $\times$  4 m (width)  $\times$  5.5 m (depth). A schematic diagram of the experimental setup is given in Fig. 1.

The sparks were initiated between two electrodes made of tungsten wires with a diameter of 1 mm. The sparker was submerged in water at a depth of 2.5 m and about 1.2 m away from the nearest tank wall. The electrodes were connected to a capacitor bank, whose capacitance  $C$  could be varied in steps by connecting 1–10 capacitors in parallel. Each of these capacitors had a capacitance of 16  $\mu$ F. The capacitors have been charged from a high voltage source of  $V = 4$  kV and an air-gap switch has been used to trigger the discharge through the sparker. The electrical energy  $E_c$  stored at the capacitors and available for discharge is given by the formula:

$$E_c = \frac{1}{2} CV^2. \quad (1)$$

Both the spark discharge and subsequent bubble oscillations are accompanied by intensive optic (thermal) and acoustic (pressure waves) radiations. These radiations have been monitored with optic and acoustic detectors. The optic detector consisted of a fiber optic cable (light guide) whose input surface has been positioned in water at the same level as the sparker at a distance of 0.2 m aside, pointing perpendicularly to the sparker gap and the electrodes. At the output surface of the fiber optic cable a photodiode has been positioned. In the experiments reported here, a Hamamatsu photodiode type S2386-18L with a usable spectral range from 320 nm to 1100 nm has been used. The load resistance of the photodiode was 75  $\Omega$ , thus the rise time, according to the manufacturer's data, was about 50 ns. And this proved to be sufficient for the experiments reported here. The frequency response of the photodiode is not constant in the given wavelength range and thus, unfortunately, it is not possible to convert the measured photodiode output voltages into radiation units. Hence the optic data will be given in voltage units referring to the photodiode output. A broadband amplifier (0–10 MHz) has been connected to the photodiode output terminals.

The acoustic radiation has been monitored with a Reson broadband hydrophone type TC 4034, having a usable frequency range from 1 Hz to 470 kHz. It has been verified, by comparison with a smaller hydrophone (Reson type TC 4038, nominal usable range from 10 kHz to 800 kHz), that the hydrophone's frequency range is sufficient to record acoustic signals radiated by large bubbles generated in experiments described here with an admissible error. This error is negligible for the largest bubbles oscillating with low intensity and is less than 10% for the smallest bubbles oscillating with high intensity. The hydrophone has been positioned vertically in water with the sensitive element at the same depth as the sparker. The distance between the hydrophone acoustic centre and the sparker gap was 0.2 m.

The output voltages from the photodiode and hydrophone have been simultaneously recorded using a data acquisition board (National Instruments PCI 6115, 12 bit A/D converter) with a sampling frequency of 10 MHz.

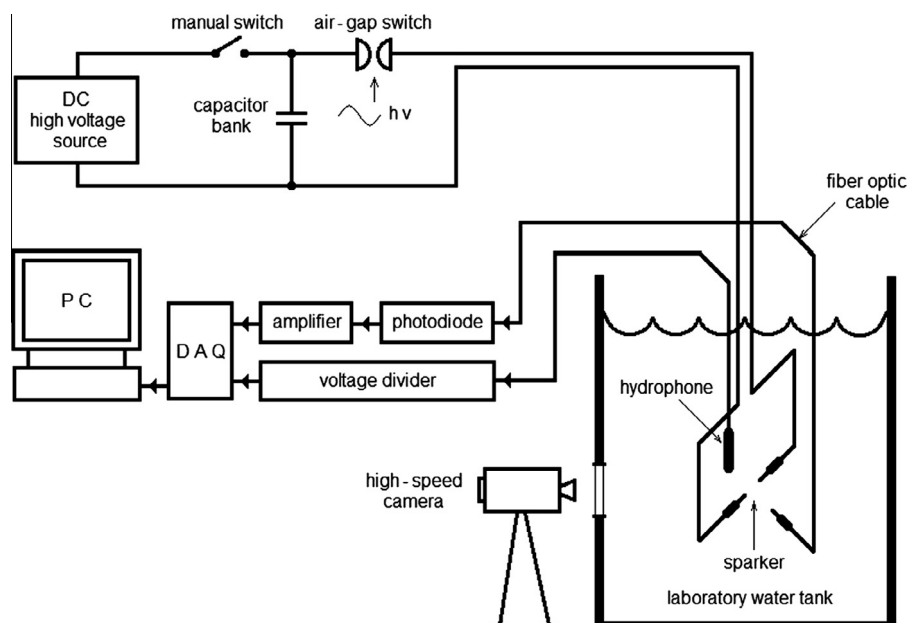


Fig. 1. Experimental setup used to generate oscillating bubbles and record optic and acoustic radiations from them. (DAQ – data acquisition board, hv – high voltage).

A limited number of high-speed camera records have been taken with framing rates ranging from 2800 to 3000 frames/s. These records have been used to check the shape of the generated bubbles (it has been verified that the bubbles retained almost spherical shapes in the vicinity of the first and second maximum radius) and the photographs yielded also useful visual information on the bubble thermal behavior. A more detailed description of the experimental setup is given in earlier works [25,26].

### 3. Generating the bubble

When a charged capacitor bank is connected to a sparker submerged in water, after a short time a liquid breakdown occurs [25]. Between the two sparker electrodes a conductive channel is formed and a discharge current flowing through it starts intensive heating of the plasma in the channel. The discharge current has a form of a highly damped sinusoid which after a short time becomes extinct [25].

Immediately following liquid breakdown, the physical processes in the discharge channel are very complex. The experimental data given in literature [28–30] indicate that the temperature of the plasma in the channel violently increases. This temperature growth is accompanied by a fast growth of pressure in the discharge channel. The plasma heated to a high temperature is a source of intensive thermal radiation with a spectral maximum lying, in these initial instants, in the near ultraviolet region. The intensive thermal radiation is partially absorbed in a liquid layer adjacent to the channel wall. This liquid layer is thus heated, evaporated, dissociated and ionized [22,24,28,29].

Due to high overpressure in the plasma, the discharge channel starts expanding explosively. And even if the initial channel shape is most probably close to a cylinder, it will be assumed here, just for the simplicity of the following discussion, that the initial channel shape at  $t = 0$  is close to a sphere of radius  $R_{m0}$  [31].

As said above, during the first instants after the liquid breakdown the explosive channel growth is driven both by the overpressure in the heated plasma and by evaporation of the liquid layer contiguous to the channel wall. However, it can be expected that the channel growth due to evaporation will soon lose its significance, as compared with forces due to overpressure. During the initial phase, an explosively expanding bubble with a nearly spherical shape and filled with high pressure and high temperature plasma is formed. And this initial bubble is a source of intensive thermal radiation, which can be considered to be blackbody radiation. The overpressure in the discharge channel and the fast motion of the channel wall are the cause that a strong pressure wave is radiated.

The time, when the intensity of the thermal radiation (as determined in the photodiode output voltage) attains a maximum value  $u_{M0}$ , will be denoted as  $t_{M0}$ . At this time the bubble radius will be  $R_{M0}$  and the surface temperature of the glowing plasma sphere  $\Theta_{M0}$ . After attaining the radius  $R_{M0}$  the bubble continues expanding till the first maximum radius  $R_{M1}$ . At this time,  $t_1$ , the surface temperature of the hottest plasma core at the bubble centre attains a value  $\Theta_{m1}$ . However, because the pressure in the expanded bubble is low, the plasma cannot be considered to radiate as a blackbody in the vicinity of the maximum radius  $R_{M1}$  anymore.

Now the bubble compression phase starts, during which the bubble is, at time  $t_{m1}$ , reduced to the first minimum volume (it will be assumed here that it is a sphere of radius  $R_{m1}$ ), and the plasma surface temperature reaches a value  $\Theta_{M1}$  and pressure  $P_{M1}$ . Because the temperature  $\Theta_{M1}$  and pressure  $P_{M1}$  are relatively high, the blackbody radiation from the bubble can be assumed in the vicinity of  $t_{m1}$  again. The two phases of the bubble growth and compression represent the first bubble oscillation of duration  $T_{o1}$ .

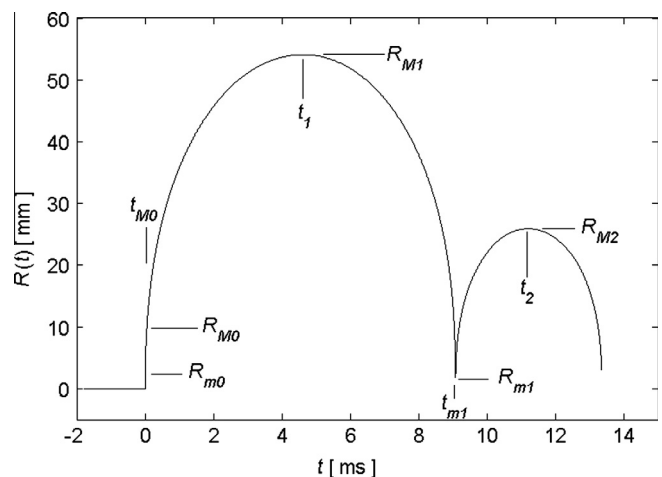


Fig. 2. A sketch showing symbols used to denote the significant bubble wall radii and corresponding time instants.

In further instants the bubble expands to a second maximum radius  $R_{M2}$ . The bubble continues its oscillatory motion during which the expansion and compression phases repeat several times. However, the intensity of the following oscillations is rapidly decreasing and the bubble also loses its spherical shape soon [26]. The bubble radii and corresponding instants just introduced are schematically shown in Fig. 2.

### 4. Results and discussion

#### 4.1. Radiated waveforms

As already mentioned, the initial discharge and the following oscillatory bubble motion are accompanied by an intensive optic and acoustic radiation. An example of a photodiode output voltage  $u(t)$  is given in Fig. 3, and an example of the corresponding pressure wave  $p(t)$  obtained with the hydrophone is given in Fig. 4.

As can be seen, both records consist of initial pulses  $u_0(t)$  and  $p_0(t)$ , radiated during the discharge and the following explosive bubble growth, and of the first pulses  $u_1(t)$  and  $p_1(t)$ , radiated during the first bubble compression and the following bubble expansion.

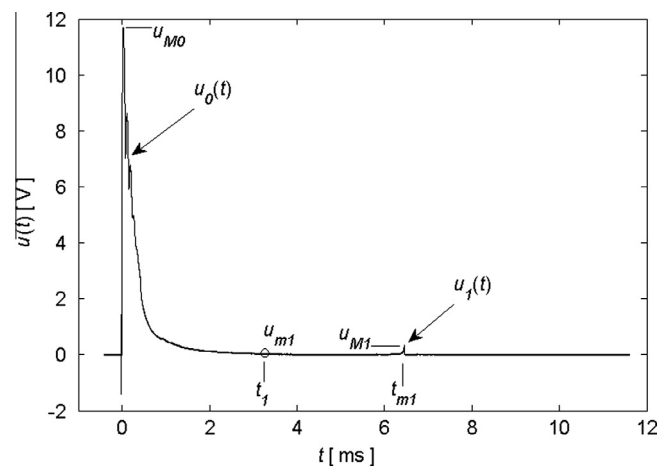
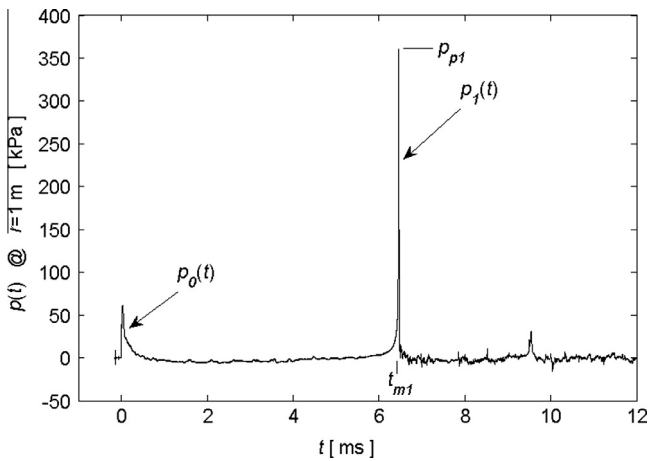


Fig. 3. An example of a radiated optic waveform  $u(t)$ . Here  $u_0(t)$  is the initial pulse radiated during the discharge, and  $u_1(t)$  is the first pulse radiated during the bubble compression.



**Fig. 4.** An example of a radiated acoustic waveform  $p(t)$ . Here  $p_o(t)$  is the initial pulse radiated during the discharge, and  $p_1(t)$  is the first pulse radiated during the bubble compression.

In both records the time origin has been selected to coincide with the instant when the pulses  $u_o(t)$  and  $p_o(t)$  start growing. In the case of the optic record, the time origin thus coincides with the liquid breakdown (and the start of the bubble growth), while in the case of the acoustic record, the time origin corresponds to the beginning of the spark discharge plus a travel time of the pressure wave from the spark gap to the hydrophone. The interval between the time origin and the first pulse peak represents the time of the first bubble oscillation  $T_{o1}$ .

To keep the extent of this paper in a reasonable size, the analysis of the acoustic pressure records will not be described, as it can be found in earlier works [25,26]. Thus, using the iterative procedure introduced in the work [26], all the pressure records have been processed to determine the bubble sizes, as represented by the maximum radii  $R_{M1}$ , and bubble oscillation intensities, as represented by a non-dimensional peak pressures in the first pulse,  $p_{zp1} = p_{p1} r_h / (p_\infty R_{M1})$ , where  $p_{p1}$  is the peak pressure in the pulse  $p_1(t)$ ,  $p_\infty$  is the ambient (hydrostatic) pressure at the place of the sparker, and  $r_h$  is the hydrophone distance from the sparker centre. And using the procedure described in detail elsewhere [25], acoustic energies carried away in the initial pressure pulse  $E_{ap0}$  and in the first pressure pulse  $E_{ap1}$  have been also calculated from the acoustic pressure records.

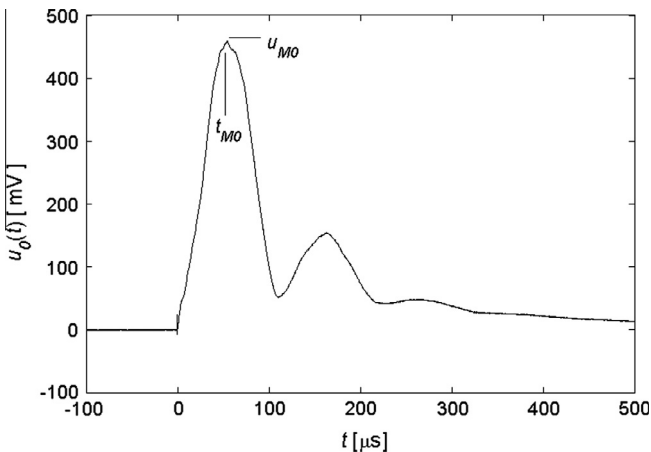


**Fig. 5.** A detailed view at the radiated initial optic pulse  $u_o(t)$ . The maximum value in the pulse, which corresponds to the maximum intensity of the optic radiation, has been denoted  $u_{M0}$ , and this value occurs at a time  $t_{M0}$ .

A detailed view at the initial optic pulse  $u_o(t)$  is given in Fig. 5. In Fig. 5 the maximum value in the initial pulse  $u_o(t)$  has been denoted as  $u_{M0}$ . And as already mentioned above, the instant the voltage attains this maximum value  $u_{M0}$  is denoted as  $t_{M0}$ .

The dynamic range of the optic detector (the photodiode, amplifier, A/D converter) was not sufficiently high to record both  $u_o(t)$  and  $u_1(t)$  in one experiment with a good fidelity. In the case the initial pulse  $u_o(t)$  was to be recorded undisturbed by an apparatus saturation, the first pulse  $u_1(t)$  was usually hidden in noise. In the case the first pulse  $u_1(t)$  was to be recorded with acceptable noise, the initial pulse  $u_o(t)$  was usually clipped (in Fig. 3 the initial pulse is slightly distorted by the apparatus saturation). Therefore two sets of experiments have been done. The first set of experiments, here denoted as set I, has been aiming at recording the initial pulse  $u_o(t)$  undisturbed, and the second set of experiments, here denoted as set II, has been aiming at recording the first pulses  $u_1(t)$  with acceptable noise. A connection between the two sets of experiments has been done by using statistical averages. Concretely, in Sections 4.6 and 4.7 the average values from the first set of records have been used to compute the respective values from the second set of records.

#### 4.2. Energy partition

In Ref. [25], the efficiency of energy conversion during bubble oscillations has been already discussed. In this work the optic (thermal) radiation from the oscillating bubble will be included in the energy partition.

The electrical energy  $E_c$  available for the discharge at the capacitor bank is given by Eq. (1). This energy is transferred into the discharge channel with an efficiency  $\eta_d$ . Thus the energy deposited into the channel,  $E_d$ , is

$$E_d = \eta_d E_c. \quad (2)$$

In Ref. [25], a mean value of the efficiency  $\eta_d$  has been determined to be  $\langle \eta_d \rangle = 0.19$  (in this paper the mean values will be denoted by angle brackets  $\langle \rangle$ ).

For the bubble growth phase  $(0, t_1)$ , the following energy balance can be written:

$$E_d = E_{op0} + E_{ap0} + E_{pM1} + E_{iM1} + E_{u0}. \quad (3)$$

Here  $E_{op0}$  is the optic energy radiated from the bubble in the initial pulse  $u_o(t)$ ,  $E_{ap0}$  is the acoustic energy radiated from the bubble in the initial pulse  $p_o(t)$ ,  $E_{pM1} = (4/3)\pi(p_\infty - P_{vp})R_{M1}^3$  is the potential energy of the bubble, when, at the end of the growth phase, the bubble has a maximum radius  $R_{M1}$ , and  $E_{iM1} = (4/3)\pi P_{vp}R_{M1}^3/(\gamma - 1)$  is the internal energy of the bubble content at  $R_{M1}$ . Here  $P_{vp}$  is the liquid vapor pressure and  $\gamma$  is the ratio of the specific heats of the bubble content. Finally in  $E_{u0}$  all energies not taken into account in Eq. (3) (e.g., heat losses due to thermal conduction) are encompassed. However, as no suitable experimental method enabling direct determination of these energies was available, the unaccounted for energies will not be considered here anymore, i.e., it will be assumed that  $E_{u0} = 0$  (it will be shown later in Section 4.4 that the unaccounted for energies must be small and therefore this assumption can be justified). On the other hand, the energies  $E_{ap0}$ ,  $E_{pM1}$  and  $E_{iM1}$  can be determined easily from the acoustics records [25] (the energies  $E_{pM1}$  and  $E_{iM1}$  are calculated from  $R_{M1}$  using the formulas given above) and hence, under the assumption done, an estimate of the optic energy can be determined from the following equation:

$$E_{op0} = \langle \eta_d \rangle E_c - E_{ap0} - E_{pM1} - E_{iM1}. \quad (4)$$

The optic energy computed in this way will be used in the following sections. However, it should be reminded here that the efficiency  $\eta_d$  is varying from one experiment to another and thus the actual value of  $E_d$  (and hence of  $E_{op0}$ ) may be different from that obtained from Eq. (4).

The energy relation for the interval  $(t_1, t_2)$ , that means for the first compression and the following expansion phases is

$$E_{pM1} + E_{iM1} = E_{op1} + E_{ap1} + E_{pM2} + E_{iM2} + E_{u1}. \quad (5)$$

Here  $E_{op1}$  is the optic energy radiated in the first pulse  $u_1(t)$ ,  $E_{ap1}$  is the acoustic energy radiated in the first pressure pulse  $p_1(t)$ ,  $E_{pM2} = (4/3)\pi(p_\infty - P_{vp})R_{M2}^3$  is the potential energy of the bubble, when, at the end of the second expansion phase, the bubble attains the second maximum radius  $R_{M2}$ ,  $E_{iM2} = (4/3)\pi P_{vp}R_{M2}^3/(\gamma - 1)$  is the internal energy of the bubble content at  $R_{M2}$ , and  $E_{u1}$  encompasses all unaccounted for energies in the interval  $(t_1, t_2)$ . In contrast to  $E_{u0}$ , which seems to be small in comparison with other terms in Eq. (3) (especially with  $E_{op0}$ ) and can be therefore neglected, the term  $E_{u1}$  is relatively large in comparison with other terms in Eq. (5) (this will be shown later in Section 4.7) and therefore cannot be neglected. Eq. (5) can be rearranged to enable determining the value of these energies not taken into account as follows:

$$E_{u1} = E_{pM1} + E_{iM1} - E_{op1} - E_{ap1} - E_{pM2} - E_{iM2}. \quad (6)$$

Again, the bubble radii  $R_{M1}$ ,  $R_{M2}$  (and thus the energies  $E_{pM1}$ ,  $E_{pM2}$ ,  $E_{iM1}$ ,  $E_{iM2}$ ) and the acoustic energy  $E_{ap1}$  can be determined from the acoustic records [25]. The way how to compute  $E_{op1}$  will be explained in the following sections.

#### 4.3. Maximum intensity of the optic radiation

During the initial explosive growth, the spherical bubble reaches very early the radius  $R_{M0}$ , for which the intensity of the optic radiation attains its maximum. Under the assumptions made earlier, this maximum intensity corresponds to the maximum voltage  $u_{M0}$ , and the instant when this occurs has been denoted as  $t_{M0}$ .

The variation of the maximum voltage  $u_{M0}$  with the maximum bubble radius,  $R_{M1}$ , is given in Fig. 6.

The regression polynomial to this data is  $\langle u_{M0} \rangle = 1.25 \times 10^{-4} R_{M1}^2$  [V, mm]. The variation of time  $t_{M0}$  with the maximum bubble radius,  $R_{M1}$ , is given in Fig. 7.

As can be seen in Fig. 7, the values of  $t_{M0}$  are ranging from about 11  $\mu\text{s}$  (small bubbles) to about 68  $\mu\text{s}$  (large bubbles). As the bubble sizes in the experiments reported here range from about 18 mm to 55 mm, then the corresponding times of the first bubble oscillations,  $T_{o1}$ , range from about 3 ms (small bubbles) to about 9 ms (large bubbles) [26]. It can be seen that in comparison with the times of the first bubble oscillation,  $T_{o1}$ , the times  $t_{M0}$  are very small (approximately  $t_{M0} = 0.005T_{o1}$ ). However, even these small times  $t_{M0}$  are sufficient for an explosively growing bubble to attain

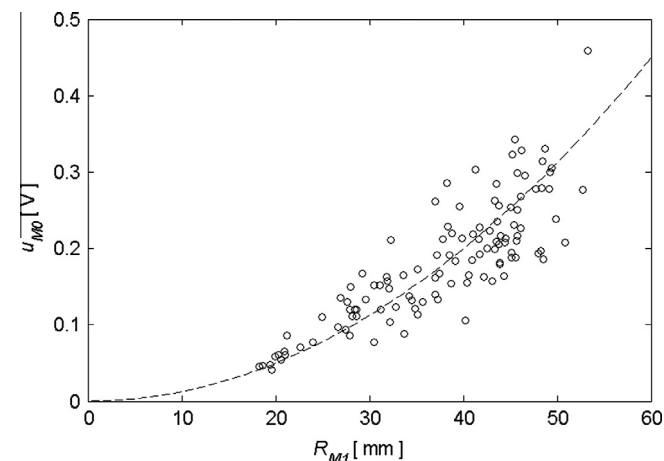


Fig. 6. Variation of the maximum value in the initial optic pulse  $u_{M0}$  with the bubble size  $R_{M1}$ .

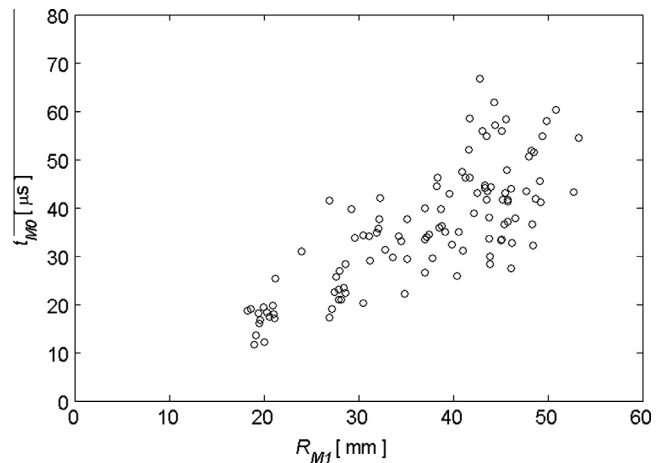


Fig. 7. Variation of the time  $t_{M0}$  at which the optic radiation attains the maximum value with the bubble size  $R_{M1}$ .

a relatively large radius  $R_{M0}$  and thus significantly influence the further bubble behavior. This special phenomenon has first been recognized by Golubnichii et al. [32]. The magnitude of  $t_{M0}$  may also differentiate the spark bubbles from the laser generated bubbles, where  $t_{M0}$  can be expected to be much smaller. The reason for this small magnitude of  $t_{M0}$  is an almost instantaneous delivery of energy into a focal point in a liquid by a laser pulse having a width typically several ns [20,33].

In the experiments reported here it was not possible to determine the values of  $R_{M0}$  directly. However, as a first order approximation, they can be computed from a theoretical variation of bubble radius  $R$  with time  $t$ . It is now necessary to point out that, at the present state of knowledge, theoretical computations of  $R$  with  $t$  in the vicinity of the minimum radii  $R_{m0}$  and  $R_{m1}$  usually give results which seem to have no solid support in experiments and hence need not to be quite correct. On the other hand, the overall shape of the curve  $R(t)$  (the so called “inverted tea cup”) is relatively “stable” for sufficiently high oscillation intensities and insensitive to the bubble oscillation intensity and any energy losses introduced into a theoretical model [34]. This is true in a relatively broad neighborhood of  $R_{M1}$  first of all. Thus, if sufficient care is taken, a suitable variation of a non-dimensional bubble radius with a non-dimensional time can be computed with a relatively simple bubble model, and then scaled to a given experimental

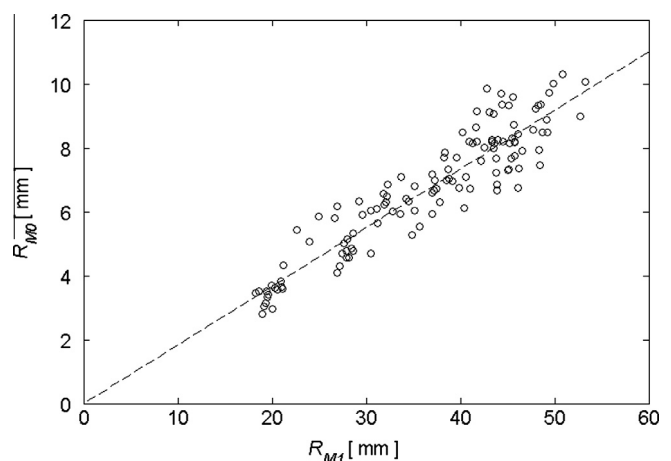


Fig. 8. Variation of the bubble radius  $R_{M0}$  at which the optic radiation attains the maximum value with the bubble size  $R_{M1}$ .

value of  $R_{M1}$  [35]. Therefore, using computed variations of  $R(t)$  (here a model described in Ref. [31] was used) and experimental values of  $R_{M1}$  and  $t_{M0}$ , the corresponding values of  $R_{M0}$  can be easily determined for each optic record  $u(t)$  from the first set of experiments. The variation of  $R_{M0}$  with  $R_{M1}$  determined in this way is given in Fig. 8. A regressive line to the variation of  $R_{M0}$  with  $R_{M1}$  is  $\langle R_{M0} \rangle = 0.1836R_{M1}$ .

#### 4.4. Radiated optic power and energy

Let us assume that the oscillating bubble thermally radiates as a blackbody. As already mentioned this is true in the vicinity of  $R_{m0}$  and  $R_{m1}$ , and it is just here where the optic radiation plays an important role. Then, according to the Stefan–Boltzmann Law, the intensity of thermal (optic) radiation from a sphere of radius  $R$  having a surface temperature  $\Theta$  is

$$H_R = \sigma \Theta^4, \quad (7)$$

where  $\sigma = 5.67 \times 10^{-8} \text{ W m}^{-2} \text{ K}^{-4}$ . Then, under the assumption of no absorption of radiation in the liquid, the intensity of thermal radiation at a distance  $r$  from a bubble of radius  $R$  is

$$H_r = \sigma \Theta^4 (R/r)^2. \quad (8)$$

Even if the photodiode is not a perfect detector (its receiving bandwidth extends only from 320 nm to 1100 nm and its sensitivity is not constant within this band), it can be assumed, as a first order approximation, that the photodiode output voltage is directly proportional to the intensity of the thermal radiation, that is

$$u = \text{const } \sigma \Theta^4 R^2 / r^2. \quad (9)$$

Then, for  $R = R_{M0}$  Eq. (9) gives

$$u_{M0} = \text{const } \sigma \Theta_{M0}^4 (R_{M0}/r)^2. \quad (10)$$

Combining Eqs. (9) and (10) yields a surface temperature  $\Theta$  of a plasma sphere of radius  $R$  if the photodiode output voltage is  $u$

$$\Theta^4 = \frac{\Theta_{M0}^4 R_{M0}^2}{u_{M0}} \frac{u}{R^2}. \quad (11)$$

The instantaneous optic power radiated from the surface of an oscillating plasma sphere of radius  $R$  is then (substituting Eq. (11) into Eq. (7)).

$$P_R(t) = H_R 4\pi R^2 = 4\pi \sigma \frac{\Theta_{M0}^4 R_{M0}^2}{u_{M0}} u(t). \quad (12)$$

The cumulative optic energy radiated from the bubble in the interval  $(0, t)$  is

$$E_o(t) = \int_0^t P_R(\tau) d\tau, \quad (13)$$

and the optic energy radiated in the initial pulse is

$$E_{op0} = 4\pi \sigma \frac{\Theta_{M0}^4 R_{M0}^2}{u_{M0}} \int_0^{t_1} u(\tau) d\tau, \quad (14)$$

and in the first pulse

$$E_{op1} = 4\pi \sigma \frac{\Theta_{M0}^4 R_{M0}^2}{u_{M0}} \int_{t_1}^{t_2} u(\tau) d\tau. \quad (15)$$

Integrals in Eqs. (14) and (15) can be computed easily from the voltage records  $u(t)$ . If  $E_{op0}$  from Eq. (4) is substituted into Eq. (14), then, for a given pair of records  $u(t)$  and  $p(t)$ , the unknown temperature  $\Theta_{M0}$  can be determined. The variation of thus obtained temperature  $\Theta_{M0}$  with the maximum bubble radius  $R_{M1}$  is given in Fig. 9.

A regression line to this variation of  $\Theta_{M0}$  with  $R_{M1}$  is  $\langle \Theta_{M0} \rangle = -0.11R_{M1} + 17.4$  [kK, mm]. Temperatures  $\Theta_{M0}$  can be used to compute the instantaneous optic power  $P_R(t)$  from Eq. (12), the cumulative optic energy  $E_o(t)$  from Eq. (13), the energy radiated in the initial optic pulse  $E_{op0}$  from Eq. (14), and the instantaneous surface temperature of the plasma  $\Theta(t)$  in the bubble growth phase from Eq. (11).

As can be seen in Fig. 9, the temperatures  $\Theta_{M0}$  range from about 10,000 to 18,000 K. These temperatures are relatively low when compared with temperatures measured by Martin [28], Robinson et al. [29], and Shvets [30]. However, these researchers have used a different discharge apparatus (higher voltage  $V$ , smaller capacitors capacitance  $C$ , smaller discharge circuit inductance  $L$ , larger discharge gaps  $d$ , exploding wire technique, etc.). On the other hand, the lower temperatures  $\Theta_{M0}$  found here may also serve as a proof that an error due to neglecting energy  $E_{u0}$  cannot be very large. This also means that in spite of enormous temperature gradients in the growing bubble, the energy losses due to thermal conduction are small. Eq. (15) has been used in Section 4.6 to compute  $E_{op1}$  in the second set of experiments.

#### 4.5. The bubble interior

In the theoretical research on bubble dynamics it is a relatively common practice to assume homogeneous temperature and pressure fields in the bubble interior [20,24,36,37]. However, a brief look at the frames taken in the experiments by a high-speed camera reveals that, for spark generated bubbles, this assumption cannot be always valid. An example of a frame taken when the bubble was in the vicinity of its maximum volume (i.e., near  $R_{M1}$ ) is given in Fig. 10.

It can be seen that the temperature field inside the bubble is by no means homogeneous. The glowing plasma core is concentrated at the centre of the bubble and the temperature, as judged by the change of the brightness at the frame, is decreasing toward the bubble wall. This decrease of the temperature toward the bubble wall might be partially due to the heat flow from the plasma into the surrounding liquid, but a more plausible explanation is that this temperature decrease is due to the thermal radiation from the plasma. High temperature plasma is opaque for thermal radiation [28], hence the radiation from the inner layers does not penetrate out of the hot core. Only the radiation from the outer layers of the plasma core penetrates into the liquid and thus, from the point of view of the bubble, it

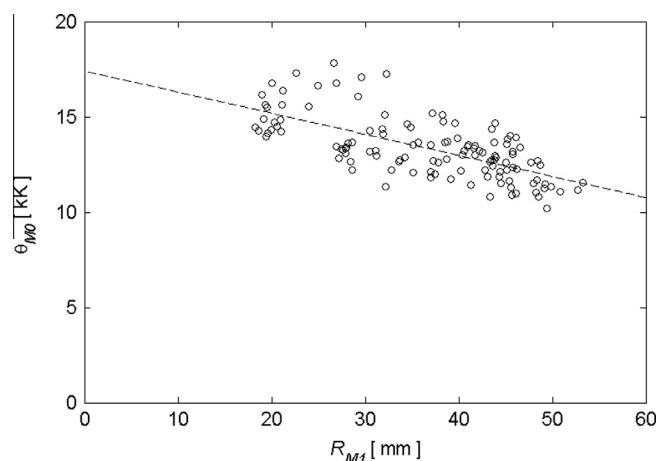
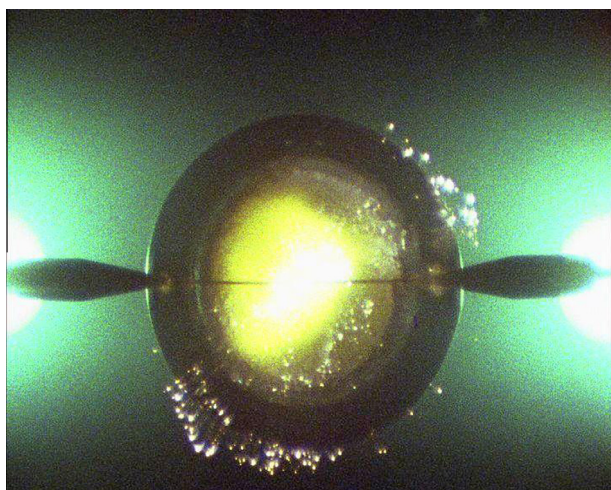


Fig. 9. Variation of the surface plasma temperature  $\Theta_{M0}$ , which corresponds to the maximum of the optic radiation from the bubble, with the bubble size  $R_{M1}$ .



**Fig. 10.** Photograph of the bubble taken near its first maximum radius  $R_{M1} = 51.5$  mm. The two tungsten electrodes and brass holders are penetrating the bubble from both sides. At the bubble centre the glowing opaque plasma core can be seen. Small bright plasma objects with tube like traces are moving in the liquid outside the bubble.

is lost. As the outer plasma layers cool down due to radiation, they become transparent and the next inner layer starts losing its energy by radiation. The assumption that the main cause of the temperature field non-homogeneity in the bubble is thermal radiation and not heat flow also follows from a remark given at the end of Section 4.4.

When determining the surface temperature of the plasma sphere, one has to take into account the surface of the opaque core at the bubble centre. In the experiments described here 10 films with a high-speed camera have been taken. The frames recorded near the maximum of the bubble volumes have been inspected visually. Although the shape of the opaque plasma core is far from being spherical, it has been substituted with a sphere of a reduced radius  $R_{M1red}$ . An average value from the 10 films is  $\langle R_{M1red} \rangle = 0.2R_{M1}$ . And this value has been used later when estimating the temperature  $\Theta_{m1}$ , i.e., when the bubble attains the maximum volume.

Small bright objects (plasma packets) in the liquid outside the bubble, which also can be seen in Fig. 10, are interesting phenomena. These objects have been observed by Golubnichii et al. [38,39] already. A closer look at Fig. 10 reveals a tube like traces behind these plasma packets. It can be suspected that these tubes are trajectories the plasma objects (packets) have travelled during the camera shuttle opening. It is also interesting that these plasma packets glow in water for a relatively long time and do not change their size and brightness (see, e.g., frames taken in different instants and displayed in Ref. [26]).

#### 4.6. Surface temperature of plasma

Eq. (11) can be used to obtain rough estimates of the temperature  $\Theta_{m1}$  (at the time  $t_1$ , when the bubble has the radius  $R_{M1}$ ), and  $\Theta_{M1}$  (at the time  $t_{m1}$ , when the bubble has the radius  $R_{m1}$ ). The photodiode output voltages corresponding to these instants have been denoted as  $u_{m1}$  (at  $t_1$ ), and  $u_{M1}$  (at  $t_{m1}$ ) in Fig. 3. To determine the time  $t_1$  it was assumed that the growth and compression phases have an equal duration, hence  $t_1 = T_{o1}/2$ .

When computing the temperatures  $\Theta_{m1}$  and  $\Theta_{M1}$  for a concrete voltage record  $u(t)$  from the second set of experiments, the average values  $\langle \Theta_{M0} \rangle$ ,  $\langle R_{M0} \rangle$ , and  $\langle u_{M0} \rangle$ , corresponding to the given radius

$R_{M1}$ , have to be used. Thus, using these averages, Eq. (11) can be written:

$$\Theta_{m1}^4 = \frac{\langle \Theta_{M0} \rangle^4 \langle R_{M0} \rangle^2}{\langle u_{M0} \rangle} \frac{u_{m1}}{\langle R_{M1red} \rangle^2}, \quad (16)$$

and

$$\Theta_{M1}^4 = \frac{\langle \Theta_{M0} \rangle^4 \langle R_{M0} \rangle^2}{\langle u_{M0} \rangle} \frac{u_{M1}}{R_{m1}^2}. \quad (17)$$

The mean value  $\langle R_{M1red} \rangle$  in Eq. (16) has been already discussed in Section 4.5. The value of the minimum radius  $R_{m1}$ , in Eq. (17), requires a brief discussion. It can be expected that its value will depend on a number of experimental parameters, as, e.g., on the bubble oscillation intensity, the method of the bubble excitation etc. This dependence is still more or less unknown. In this paper the value of  $R_{m1} = 0.03R_{M1}$ , which was determined for spark generated bubbles in Ref. [31], has been used. However, it should also be remarked that another uncertainty connected with  $R_{m1}$  concerns the time coincidence of  $R_{m1}$  and  $u_{M1}$ . It has been shown [40] that the maximum voltage  $u_{M1}$  usually does not occur at the same instant as the peak pressure in the acoustic record  $p(t)$ , i.e., when one may expect that the bubble is compressed to the minimum volume represented by the minimum radius  $R_{m1}$ . Thus the actual value of  $R_{m1}$  to be substituted into Eq. (17) should be larger and therefore the temperature  $\Theta_{M1}$  can be lower than that computed from Eq. (17), using the value of  $R_{m1}$  given above.

The values of  $\Theta_{m1}$  computed with Eq. (16) must be taken with great care as Eq. (16) has been derived under the assumption that the bubble is a blackbody radiator. However, as mentioned above, this assumption is not valid in the vicinity of  $R_{M1}$ .

#### 4.7. A concrete example

To illustrate the method used here and to present some concrete numerical results, an example of computations will be given. For this purpose two experiments were selected, one from the set I and the second from the set II. Both experiments have been done with a capacitor bank having the total capacitance  $C = 160 \mu\text{F}$  and the charging voltage of  $V = 4 \text{ kV}$ . Thus the available electrical energy, as determined from Eq. (1), is  $E_c = 1280 \text{ J}$ .

From the first set of experiments a pair of records  $u(t)$  and  $p(t)$  has been selected. In this case the bubble had the size  $R_{M1} = 53.2 \text{ mm}$  and was oscillating with intensity  $p_{zpl} = 130.0$ . These bubble parameters have been determined from the pressure record  $p(t)$  and their values confirm that the hydrophone's bandwidth was sufficient for a relatively reliable recording of the pressure wave [41]. Then from the same pressure record  $p(t)$  the acoustic energy radiated in the initial pulse  $E_{ap0}$ , the potential energy of the bubble  $E_{pM1}$ , and the internal energy of the bubble content  $E_{iM1}$  were calculated. Using the value of the mean efficiency  $\langle \eta_d \rangle$ , the energy deposited into the discharge channel  $E_d$  was computed from the electric energy  $E_c$ . Finally, using Eq. (4) the optic energy radiated in the initial optic pulse  $E_{op0}$  has been determined. All these energies associated with the time interval  $(0, t_1)$  are summarized in Table 1. In the third column of Table 1 these energies are expressed as the percentage of  $E_d$ . When computing the energies  $E_{pM1}$  and  $E_{iM1}$

**Table 1**  
Energy partition in the first bubble growth phase.

$E_d$	243.2 J	100%
$E_{op0}$	153.4 J	63.0%
$E_{ap0}$	7.0 J	2.9%
$E_{pM1}$	77.7 J	32.0%
$E_{iM1}$	5.1 J	2.1%

(and later on also the energies  $E_{pM2}$  and  $E_{iM2}$ ) the following numerical values have been used:  $p_{\infty} = 1.25 \times 10^5$  Pa,  $P_{vp} = 2$  kPa, and  $\gamma = 1.25$ .

From the record  $u_I(t)$  it was further determined that  $u_{M0} = 0.2$  V and  $t_{M0} = 30$   $\mu$ s. Using the computational procedure described in Section 4.3, it has been found that  $R_{M0} = 10.1$  mm. Then inserting the value of  $E_{op0}$  given in Table 1 into Eq. (14), and after integrating  $u_I(t)$  in interval  $(0, t_1)$ , the temperature  $\Theta_{M0} = 11,600$  K was determined (all computed temperatures are given rounded in this work). Using the values of  $\Theta_{M0}$ ,  $R_{M0}$ , and  $u_{M0}$ , time variations of temperature  $\Theta(t)$ , instantaneous optic power  $P_R(t)$ , and cumulative optic energy  $E_o(t)$  can be computed from Eqs. (11)–(13). These variations of  $\Theta(t)$ ,  $P_R(t)$ , and  $E_o(t)$  are plotted in Figs. 11 and 12 together with the theoretical variation of the bubble radius  $R(t)$ . The variation of  $R(t)$  has been computed using a bubble model described elsewhere [31], and the remarks mentioned in this respect to such a model at the end of Section 4.3 certainly apply.

To determine energies and temperatures in the time interval  $(t_1, t_2)$ , a pair of records  $u_{II}(t)$  and  $p_{II}(t)$  from the second set of experiments has been selected. This selection was based on the requirement that the two basic bubble descriptors, namely the maximum radius  $R_{M1}$  and oscillation intensity  $p_{zp1}$  have values close to the values of the same descriptors for the pair of the records selected

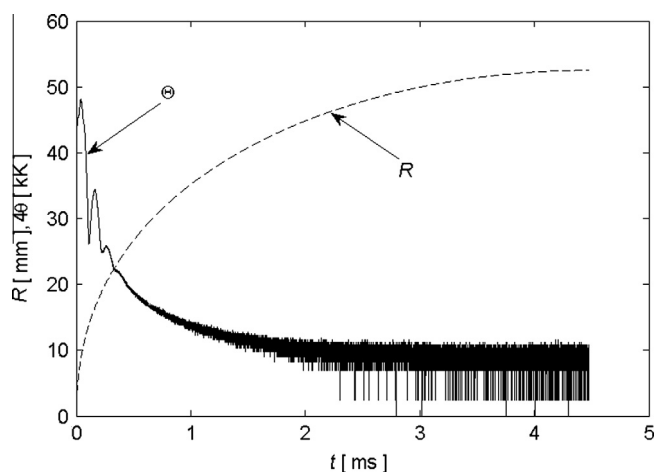


Fig. 11. Variation of the bubble radius  $R$  and plasma surface temperature  $\Theta$  with time during the growth phase.

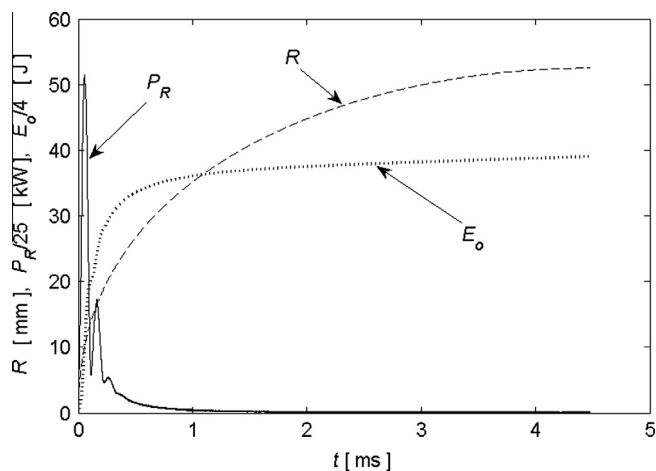


Fig. 12. Variation of the bubble radius  $R$ , instantaneous radiated optic power  $P_R$  and cumulative radiated optic energy  $E_o$  with time during the growth phase.

from the first set of experiments. Thus in the selected experiment the maximum bubble radius  $R_{M1}$ , as determined from the pressure record  $p_{II}(t)$ , was  $R_{M1} = 51.3$  mm, and the bubble oscillation intensity  $p_{zp1} = 128.3$ . From the pressure record  $p_{II}(t)$  the energies  $E_{ap1}$ ,  $E_{pM1}$ ,  $E_{iM1}$ ,  $E_{pM2}$ , and  $E_{iM2}$  were also calculated. To determine the optic quantities from the record  $u_{II}(t)$ , the average values from the first set of records has to be used. For the bubble size  $R_{M1} = 51.3$  mm the required average values are  $\langle \Theta_{M0} \rangle = 11,700$  K,  $\langle R_{M0} \rangle = 9.5$  mm, and  $\langle u_{M0} \rangle = 0.33$  V. Substituting these averages into Eq. (15) and after integrating the record  $u_{II}(t)$  in the time interval  $(t_1, t_2)$ , the optic energy  $E_{op1}$  was determined. Finally, from Eq. (6) the unaccounted for energy  $E_{u1}$  was computed. The energies thus found are summarized in Table 2. In the third column of Table 2 these energies are expressed as the percentage of  $E_{pM1} + E_{iM1}$ .

It should be said here that energy partitions based on experimental data, such as those given in Tables 1 and 2, are seldom given in the literature. Majority of researchers verify their theoretical models by fitting measured radii with a computed variation of the bubble radius with time (see, e.g., Ref. [20]). To obtain a desired agreement between measured and computed radius variations at the second bubble oscillation (i.e., in the vicinity of  $R_{M2}$ ), the initial bubble oscillation intensity is being increased as long as the energy dissipated in the theoretical model covers all the demanded energy losses. However, such an approach may lead to erroneous results. As already said, the overall shape of the bubble radius vs. time variation (the “inverted tea cup” form) is insensitive to the bubble oscillation intensity and energy dissipation. When increasing the oscillation intensity, the “inverted tea cup” corresponding to the second oscillation is decreasing its size independently of the dissipation mechanism used in the theoretical model. Thus it cannot be used for a reliable assessment of the energies involved in bubble oscillations. As can be seen in this paper and in works of other researchers (e.g., in Refs. [24,42]), physical processes in spark and laser generated bubbles are much more complex than it is assumed in relatively simple theoretical gas bubble models, used, e.g., in Ref. [20]. However, to keep the extent of the present paper in a reasonable size a detailed discussion of this topic will be published elsewhere.

Finally, the temperatures  $\Theta_{m1}$  and  $\Theta_{M1}$  can be determined using the procedure outlined in Section 4.6. The necessary average values  $\langle \Theta_{M0} \rangle$ ,  $\langle R_{M0} \rangle$ , and  $\langle u_{M0} \rangle$  were given above. The following values of the bubble radii were used:  $\langle R_{M1red} \rangle = 0.2R_{M1}$ , and  $R_{m1} = 0.03R_{M1}$ . The values of  $u_{m1} = 0.114$  mV and  $u_{M1} = 0.553$  mV were taken from the record  $u_{II}(t)$ . The computed radii and temperatures are summarized in Table 3.

Table 2

Energy partition in the first bubble compression and the following expansion phases.

$E_{pM1}$	69.5 J	93.9%
$E_{iM1}$	4.5 J	6.1%
$E_{pM1} + E_{iM1}$	74.0 J	100%
$E_{op1}$	0.8 J	1.1%
$E_{ap1}$	30.4 J	41.0%
$E_{pM2}$	6.0 J	8.1%
$E_{iM2}$	0.4 J	0.5%
$E_{u1}$	36.5 J	49.3%

Table 3

Significant bubble wall radii and corresponding plasma surface temperatures.

$\langle R_{M0} \rangle$	9.5 mm	$\langle \Theta_{M0} \rangle$	11,700 K
$R_{M1}$	51.3 mm	–	–
$\langle R_{M1red} \rangle$	10.3 mm	$\Theta_{m1}$	1500 K
$R_{m1}$	1.5 mm	$\Theta_{M1}$	5900 K
$R_{M2}$	22.6 mm	–	–

Before closing this section a few remarks should be given. It is evident that the computed values, especially those related to the second set of experiments, represent the first order estimates only. This is due to the fact that the average values of  $\langle \Theta_{M0} \rangle$ ,  $\langle R_{M0} \rangle$ , and  $\langle u_{M0} \rangle$  determined on the first set of experiments have been used. Further assumptions concern  $E_{iM1}$ ,  $E_{iM2}$  (these energies have been computed from a formula valid for an adiabatic bubble), the mean values  $\langle \eta_d \rangle$ ,  $\langle R_{M1red} \rangle$ ,  $R_{m1}$ , and putting  $E_{i0} = 0$ . However, despite so many simplifications, it seems that the results presented in Tables 1–3 are not too far from reality. The values of temperature given in Table 3 can also be compared with results found in the literature. Golubnichii et al. [38,39] have measured an optic spectrum radiated by a spark generated bubble at  $R_{M1}$  and fitted it with a blackbody spectrum corresponding to the temperature  $\Theta_{m1} = 2850$  K. These authors have shown that the measured spectrum coincides with the blackbody spectrum in a limited wavelength range only. This shows that the bubble does not radiate as a blackbody in the vicinity of the maximum radius  $R_{M1}$ . Lu et al. [24], using a theoretical model, arrived at the value of  $\Theta_{m1} = 2900$  K for a spark generated bubble. For laser generated bubbles Baghdassarian et al. [33] have experimentally determined that  $\Theta_{M1} = 7800$  K. For a spark generated bubble Lu et al. [24] computed the value of  $\Theta_{M1} = 12,000$  K. Finally, Byun et al. [42], using a theoretical model of a laser generated bubble, have calculated temperatures corresponding to the first bubble compression ranging from  $\Theta_{M1} = 7100$  to  $7800$  K. It can also be interesting to compare the results given in Table 1 with the results obtained for spark generated bubbles in Refs. [22,24,37], and for laser generated bubbles in Ref. [23]. Such a comparison reveals large differences between the results of these researchers and the results given here. In all the works mentioned, the energy  $E_{opp0}$  is considered to be very small. And, on the contrary, the energy  $E_{app0}$  is assumed to be large. The results presented here are thus just opposite to those findings. It is evident that in order to be able to explain these differences, further measurements and analyzes are needed.

#### 4.8. Adiabatic assumption

In this Section it will be shown that the adiabatic assumption is not valid for the spark generated bubbles. It will be assumed for a moment that the oscillating bubble contains a non-condensable gas in its interior and the bubble expansion and compression can be considered to be adiabatic, which means there are no thermal radiation from the bubble and no heat flow between the gas and the surrounding liquid. Further it will be assumed that the temperature is distributed homogeneously within the bubble interior. Then the temperature  $\Theta_{M0}$ , which corresponds to the bubble radius  $R_{M0}$ , can be related to a temperature  $\Theta$ , corresponding to a bubble of radius  $R$ , by a simple relation

$$\Theta = \Theta_{M0} \left( \frac{R_{M0}}{R} \right)^{3(\gamma-1)}, \quad (18)$$

Here  $\gamma$  is the ratio of the specific heats of the non-condensable gas inside the bubble. Using Eq. (18), a couple of simple computations can be done. For this purpose, it will be assumed that a bubble has a maximum radius  $R_{M1} = 51.3$  mm. Then (see Table 3)  $R_{M0} = 9.5$  mm and  $R_{m1} = 1.5$  mm. If it is further assumed that  $\Theta_{M0} = 11,700$  K and  $\gamma = 1.25$ , then, according to Eq. (18), the temperature corresponding to  $R_{M1}$  should be  $\Theta_{m1} = 3300$  K and the temperature corresponding to  $R_{m1}$  should be  $\Theta_{M1} = 46,800$  K. It can be immediately seen that these two temperatures differ from those computed in the preceding section and given in Table 3. This is true especially for the temperature  $\Theta_{M1}$ . This difference is certainly not surprising. As it has been shown above, the bubble undergoes an intensive thermal radiation during the growth phase.

However, a surprising fact is that the bubble appears not to behave adiabatically even in the compression phase, when the thermal radiation can be neglected. The bubble behavior in the compression phase shows even larger deviations from the adiabatic assumption than in the growth phase. It should be recalled here that the unaccounted for energies (Table 2) at time  $t_2$  ( $R_{M2}$ ) represent as much as 50.6% of the energy available at  $R_{M1}$ . Thermal radiation is negligible in the compression phase (1.1%). Heat losses due to thermal conduction must also be small in the compression phase. This follows from the fact that no heat losses due to thermal conduction have been considered during the growth phase, where, at least at the beginning of this phase, the temperature gradients are enormous. A possible candidate for the unaccounted for energy losses in the compression and the following expansion phases is liquid evaporation. In the vicinity of  $R_{m1}$  the pressure and temperature in the bubble interior are above the critical point of water and thus the liquid at the bubble wall might evaporate extremely fast. In this way a significant part of the internal energy could be lost. However, no direct experimental evidence for this is known at present time and thus the unaccounted for energies still remain a bit mysterious.

The above discussion is not meant to say that the adiabatic assumption is totally useless. Its advantage is a relative simplicity and thus, when carefully used and interpreted, it can facilitate the understanding of some processes. For example, when computing the bubble wall motion in the vicinity of the bubble maximum radius  $R_{M1}$ , it seems that the adiabatic assumption can yield reasonable results. However, its application in the regions near the minimum radii  $R_{m0}$  and  $R_{m1}$  can yield very erroneous values, and thus great care must be taken when interpreting these computations.

This section can be concluded by noting that according to the experimental data, the spark generated bubble does not behave adiabatically. On the contrary, its oscillations are accompanied by intensive thermal radiation and hence by intensive heat losses. This assertion is valid for the first bubble oscillation first of all. As far as the further bubble oscillations (second, third, etc.) are concerned, the lack of reliable experimental data prevents drawing any valid conclusion at present time.

## 5. Conclusions

In the paper the thermal behavior of the spark generated bubbles has been studied. The analysis has been based on the experimental data obtained by means of optic and acoustic sensors, and partially also a high speed camera. It has been shown that the interior of the spark generated bubbles is filled with high temperature plasma during the first oscillation. As a parallel to the established names “gas bubble” and “vapor bubble” it is therefore suggested to call the spark generated bubble “plasma bubble”. It has been shown that the spark generated bubbles do not behave adiabatically. Moreover, the temperature inside the bubble is not distributed homogeneously and the plasma is not in thermal equilibrium. Its description by means of the equation of state is therefore not possible. The temperatures of the plasma surface determined here seem to be in a relatively good agreement with the results of other researchers. The temperatures corresponding to the instants of the maximum intensity of the thermal radiation range between 10,000 and 18,000 K. These values are lower than the temperatures found for spark discharges in water by other researchers. The difference is, most probably, due to a slower discharge process in experiments described here. In a concrete example, the surface temperature of the hot plasma core, when the bubble attains its first maximum volume, was found to be 1500 K. However, as has already been mentioned several times, this value must be taken with great care. The surface temperature of the plasma, when the bubble is compressed to its first minimum

volume, was, in the concrete experiment described earlier, 5900 K. The energy partition during the first bubble growth phase indicates that the thermal conduction, in spite of enormous temperature gradients, does not play any important role in the case of relatively large bubbles studied here. However, a large part of the energy stored in the plasma is carried away from the bubble in a form of thermal radiation. As it can be expected, thermal radiation is not important in the first bubble compression phase. In this phase, however, the analysis reveals very large energy losses, whose character is not clear yet. The analyzes in this work have concentrated on the important question of the spark bubble thermal behavior primarily. The light emission from the bubble during its first compression has been omitted purposefully, as it is planned to deal with it in a greater detail elsewhere. And similarly it is intended to analyze the complex initial phase of the bubble formation in a greater detail elsewhere. The results reported here have been obtained when studying the spark generated bubbles. Thus, strictly speaking, they are valid for the spark generated bubbles only. However, we believe that they may help to a better understanding of other types of bubbles, such as those generated by laser, or bubbles oscillating in acoustic resonators.

### Acknowledgments

This work has been partly (K.V.) supported by the Ministry of Education of the Czech Republic as the research project MSM 467 478 8501. The authors also wish to thank Dr. Silvano Buogo from the Italian Acoustics Institute, CNR, Rome, Italy, for a very valuable help in preparing the experiments.

### References

- [1] T.G. Leighton, *The Acoustic Bubble*, Academic Press, London, 1994 (Chapter 5.4).
- [2] F.R. Young, *Cavitation*, Imperial College Press, London, 1999 (Chapters 4.13 and 8).
- [3] P.A. Dayton, J.S. Allen, K.W. Ferrara, The magnitude of radiation force on ultrasound contrast agents, *J. Acoust. Soc. Am.* 112 (2002) 2183–2192.
- [4] H.J. Vos, F. Guidi, E. Boni, P. Tortoli, Method for microbubble characterization using primary radiation force, *IEEE Trans. Ultrason. Ferroelectr. Freq. Control* 54 (2007) 1333–1344.
- [5] E.P. Stride, C.C. Coussios, Cavitation and contrast: the use of bubbles in ultrasound imaging and therapy, *Proc. Inst. Mech. Eng. J. Eng. Med.* 224 (2010) 171–191.
- [6] E. Barlow, A.J. Mulholland, A. Gachagan, A. Nordon, Theoretical investigation of chirp insonification of ultrasound contrast agents, *Ultrasonics* 51 (2011) 725–733.
- [7] J. Sijl, H.J. Vos, T. Rozendal, N. de Jong, D. Lohse, M. Versluis, Combined optical and acoustical detection of single microbubble dynamics, *J. Acoust. Soc. Am.* 130 (2011) 3271–3281.
- [8] L. Stricker, A. Prosperetti, D. Lohse, Validation of an approximate model for the thermal behavior in acoustically driven bubbles, *J. Acoust. Soc. Am.* 130 (2011) 3243–3251.
- [9] K. Uchida, S. Suzuki, A study on the hydrodynamic load in a water pool when discharged air forms a bubble cloud, *J. Press. Vess. Technol.* 129 (2007) 567–575.
- [10] J.J. Cor, T.F. Miller, Theoretical analysis of hydrostatic implodable volumes with solid inner structures, *J. Fluid Struct.* 25 (2009) 284–303.
- [11] C. Frez, G.J. Diebold, Laser generation of gas bubbles: photoacoustic and photothermal effects recorded in transient grating experiments, *J. Chem. Phys.* 129 (2008) 184506.
- [12] C. Devin, Survey of thermal, radiation, and viscous damping of pulsating air bubbles in water, *J. Acoust. Soc. Am.* 31 (1959) 1654–1667.
- [13] R. Hickling, Effects of thermal conduction in sonoluminescence, *J. Acoust. Soc. Am.* 35 (1963) 967–974.
- [14] R.B. Chapman, M.S. Plesset, Thermal effects in the free oscillation of gas bubbles, *Trans. ASME J. Basic Eng.* 93 (1971) 373–376.
- [15] A. Prosperetti, Thermal effects and damping mechanisms in the forced radial oscillations of gas bubbles in liquids, *J. Acoust. Soc. Am.* 61 (1977) 17–27.
- [16] R.I. Nigmatulin, N.S. Khabeev, F.B. Nagiev, Dynamics, heat and mass transfer of vapour-gas bubbles in a liquid, *Int. J. Heat Mass Transfer* 24 (1981) 1033–1044.
- [17] L.A. Crum, The polytropic exponent of gas contained within air bubbles pulsating in a liquid, *J. Acoust. Soc. Am.* 73 (1983) 116–120.
- [18] A. Prosperetti, The thermal behaviour of oscillating gas bubbles, *J. Fluid Mech.* 222 (1991) 587–616.
- [19] M.A. Ainslie, T.G. Leighton, Review of scattering and extinction cross-sections, damping factors, and resonance frequencies of a spherical gas bubble, *J. Acoust. Soc. Am.* 130 (2011) 3184–3208.
- [20] W. Lauterborn, T. Kurz, Physics of bubble oscillations, *Rep. Prog. Phys.* 73 (2010) 106501.
- [21] K. Vokurka, Amplitudes of free bubble oscillations in liquids, *J. Sound Vib.* 141 (1990) 259–275.
- [22] R.M. Roberts, J.A. Cook, R.L. Rogers, A.M. Gleeson, T.A. Griffy, The energy partition of underwater sparks, *J. Acoust. Soc. Am.* 99 (1996) 3465–3475.
- [23] A. Vogel, J. Noack, K. Nahen, D. Theisen, S. Busch, U. Parlitz, D.X. Hammer, G.D. Noojin, B.A. Rockwell, Energy balance of optical breakdown in water at nanosecond to femtosecond time scales, *Appl. Phys. B Lasers Opt.* 68 (1999) 271–280.
- [24] X. Lu, Y. Pan, K. Liu, M. Liu, H. Zhang, Spark model of pulsed discharge in water, *J. Appl. Phys.* 91 (2002) 24–31.
- [25] S. Buogo, J. Plocek, K. Vokurka, Efficiency of energy conversion in underwater spark discharges and associated bubble oscillations: experimental results, *Acust. Acta Acust.* 95 (2009) 46–59.
- [26] S. Buogo, K. Vokurka, Intensity of oscillation of spark-generated bubbles, *J. Sound Vib.* 329 (2010) 4266–4278.
- [27] K. Vokurka, S. Buogo, Is thermal behavior of spark generated bubbles adiabatic?, in: H. Hanselka (Ed.), on the CD-ROM: Collected papers, 38 Jahrestagung für Akustik, DAGA 2012, Darmstadt, March 19–22, 2012, pp. 871–872, (available from Deutsche Gesellschaft für Akustik, Berlin, ISBN: 978-3-939296-04-1), <<http://www.kfy.tul.cz/vyzkum/publikace/publikace-clenu-katedry/78-vokurka>> (date last viewed 03.03.2013).
- [28] E.A. Martin, Experimental investigation of a high-energy density, high-pressure arc plasma, *J. Appl. Phys.* 31 (1960) 255–267.
- [29] J.W. Robinson, M. Ham, A.N. Balaster, Ultraviolet radiation from electrical discharges in water, *J. Appl. Phys.* 44 (1973) 72–75.
- [30] I.S. Shvets, On the determination of the specific electrical conductivity of an underwater spark discharge plasma (in Russian), *Teplotf. Vys. Temp.* 18 (1980) 1–8.
- [31] K. Vokurka, A model of spark and laser generated bubbles, *Czech J. Phys.* B38 (1988) 27–34.
- [32] P.I. Golubnichii, V.M. Gromenko, A.D. Filonenko, Recombination mechanism for emission accompanying collapse of a cavitation bubble induced by a high-voltage electrical discharge (in Russian), *Zh. Tekh. Fiz.* 52 (1982) 1966–1971.
- [33] O. Baghdassarian, H.-C. Chu, B. Tabbert, G.A. Williams, Spectrum of luminescence from laser-created bubbles in water, *Phys. Rev. Lett.* 86 (2001) 4934–4937.
- [34] K. Vokurka, On rayleigh's model of a freely oscillating bubble. II. Results, *Czech J. Phys.* B35 (1985) 110–120.
- [35] K. Vokurka, The scaling law for free oscillations of gas bubbles, *Acustica* 60 (1986) 269–276.
- [36] J.A. Cook, A.M. Gleeson, R.M. Roberts, R.L. Rogers, A spark-generated bubble model with semi-empirical mass transport, *J. Acoust. Soc. Am.* 101 (1997) 1908–1920.
- [37] I.V. Timoshkin, R.A. Fouracre, M.J. Given, S.J. MacGregor, Hydrodynamic modelling of transient cavities in fluids generated by high voltage spark discharges, *J. Phys. D Appl. Phys.* 39 (2006) 4808–4817.
- [38] P.I. Golubnichii, V.M. Gromenko, V.M. Krutov, Formation of long-lived luminescent objects under decomposition of a dense low-temperature water plasma (in Russian), *Zh. Tekh. Fiz.* 60 (1990) 183–186.
- [39] P.I. Golubnichii, V.M. Gromenko, Ju.M. Krutov, Long-lived luminescent formations inside pulsating cavern initiated by powerful energy emission in water (in Russian), *Dok. Akad. Nauk SSSR* 311 (1990) 356–360.
- [40] K. Vokurka, S. Buogo, Experimental study of light emission from spark generated bubbles, in: M. Möser, B. Schulte-Fortcam, M. Ochmann, DAGA 2010, Berlin, March 15–18, 2010, pp. 671–672 (available from Deutsche Gesellschaft für Akustik, Berlin, ISBN: 978-3-9808659-8-2), <<http://www.kfy.tul.cz/vyzkum/publikace/publikace-clenu-katedry/78-vokurka>> (date last viewed 03.03.2013).
- [41] K. Vokurka, S. Buogo, A minimum hydrophobic bandwidth for undistorted cavitation noise measurement, in: M. Brothánek, R. Svobodová (Eds.), Proceedings of the 76th Acoustic Seminar, Hodonín, Czech Republic, May 13–15, 2008, pp. 99–108 (available from Czech Acoustical Society, Prague, ISBN: 978-80-01-04078-2), <<http://www.kfy.tul.cz/vyzkum/publikace/publikace-clenu-katedry/78-vokurka>> (date last viewed 03.03.2013).
- [42] K.-T. Byun, H.-Y. Kwak, S.W. Karng, Bubble evolution and radiation mechanism for laser-induced collapsing bubble in water, *Jpn. J. Appl. Phys.* 43 (2004) 6364–6370.